Molecular dynamics studies of entangled polymer chains

Bulacu, Monica Iulia

Chapter 4

Polymer melt dynamics

Books are not made to be believed, but to be subjected to inquiry.

Umberto Eco

Extensive molecular dynamics simulations have been performed to study the effect of chain conformational rigidity, controlled by bending and torsion potentials, on self-diffusion in polymer melts. The polymer model employs a novel torsion potential that avoids computational singularities without the need to impose rigid constraints on the bending angles. Two power laws are traditionally used to characterize the dependence of the self-diffusion coefficient on polymer length: $D \propto N^{-\nu}$ with $\nu = 1$ for $N < N_{\mathrm{e}}$ (Rouse regime) and with $\nu = 2$ for $N > N_{\mathrm{e}}$ (reptation regime), N_{e} being the entanglement length. Our simulations, at constant temperature and density, up to $N = 250$ reveal that, as the chain rigidity increases, the exponent ν gradually increases towards $\nu = 2.0$ for $N < N_{\mathrm{e}}$ and $\nu = 2.2$ for $N > N_{\mathrm{e}}$. The value of N_{e} is slightly increased from 70 for flexible chains, up to the point where the crossover becomes undefined. This behavior is confirmed also by an analysis of the bead mean-square displacement. Subsequent investigations of the Rouse modes, dynamical structure factor and chain trajectories indicate that the pre-reptation regime, for short stiff chains, is a modified Rouse regime rather than reptation.

[0]Based on *Effect of bending and torsion rigidity on self-diffusion in polymer melts: A molecular dynamics study*, Monica Bulacu and Erik Van der Giessen, J. Chem. Phys., 123, 114901 (2005).

4.1 Introduction

Examples of polymers can be found everywhere in our life, from DNA and proteins to plastics. The rigidity of these natural or synthetic polymers plays an important role in their dynamics, with enormous consequences for biological functions and for plastics processing or reliability.

The dynamics of polymer chains in a melt is a complex multi-body problem that has to take into account the entanglements of the chains and their time fluctuations, the cooperative bead motion as well as the particular behavior of the different chain parts during motion.

Two of the most widely used theories for polymer melt dynamics reduce the problem to a single chain motion in an effective medium: the *Rouse model* for the simple case of unentangled chains (Rouse 1953) and the *reptation model* for entangled chains (de Gennes 1979, Doi and Edwards 1989). In the Rouse model, a Gaussian chain of beads connected by springs interacts with a stochastic medium that mimics the presence of the other chains. As a consequence, the chain center of mass is subjected to particle-like diffusion and the self-diffusion coefficient D scales with the chain length N as $D \propto N^{-1}$. In the reptation model, the polymer chain is confined inside a "tube" formed by the constraints imposed by the entanglements with other chains. One of the main predictions of this theory is the N^{-2} scaling of the self-diffusion coefficient for chains that are long enough to entangle, i.e. $N > N_{\mathrm{e}}$, the entanglement length.

Starting from this classical dichotomy, melt dynamics theory has recently developed into different directions: improved versions of reptation theory (Rubinstein 1987, des Cloizeaux 1988, Frischknecht and Milner 2000); mode-coupling theory for one chain (Schweizer 1989); many-chain microscopic theory (Guenza 1999). All of the referenced theories usually find $D \propto N^{-\nu}$ with $\nu = 2$ or even stronger, $\nu = 2.25$ (Frischknecht and Milner 2000).

Interestingly, also in recent experimental work and by re-interpretation of older experimental data (Lodge 1999, Tao et al. 2000, Wang 2003, von Meerwall et al. 1998, von Meerwall et al. 2003), it was found that $\nu > 2$ for the total range of polymer lengths investigated without any crossover to $\nu = 1$ scaling for short chains. However, the experimental results do not have a straightforward interpretation due to possible glass-transition and polydispersity effects.

Given the current situation, computer simulations can bring more insight into chain dynamics by means of a better control of parameters (monodispersity, iso-friction) and through the possibility of analyzing in detail the motion of every bead or chain in the polymer melt. The only restriction is that the required simulation time for extracting the transport coefficients in melts with long chains is limited by the available computer power. Within the current limits, several numerical simulations have been performed

recently to compute the self-diffusion coefficient and to capture its scaling law as a function of chain length.

One of the early Monte Carlo (MC) simulations of a dense diamond lattice system of entangled polymer chains determined $D \propto N^{-2.1}$ over a wide density range, without any crossover from Rouse to reptation regime (Kolinski et al. 1987a). Soon after that, using MC simulation of longer chains confined to a cubic lattice, the same authors (Kolinski et al. 1987b) found a crossover from a relatively weak $N^{-1.56}$ dependence to a much stronger one $D \propto N^{-2.04}$ at $N_\mathrm{e} \approx 125$. Subsequent MC simulations (Paul et al. 1991, Shaffer 1994), however, identified a crossover between the $D \propto N^{-1}$ and the $D \propto N^{-2}$ regimes at N_e between 20 and 40.

In a seminal study, Kremer and Grest (1990) performed coarse-grained molecular dynamics (MD) simulations of polymer melts and the results indicate an entanglement length $N_\mathrm{e} \approx 35$ at which $\nu = 1.1$ changes to almost $\nu = 2$. Later, in an improved reanalysis, Pütz et al. (2000) found $N_\mathrm{e} \approx 30$ from bead mean-square displacement and $N_\mathrm{e} \approx 70$ from diffusion coefficient dependence on chain length.

The Kremer-Grest model was also used recently to investigate the influence of chain stiffness on melt dynamical properties and the results were found to be strongly influenced by the inclusion of a bending potential (Faller and Müller-Plathe 2001, Everaers et al. 2004). The authors conclude that as the stiffness increases, N_e decreases and reptation characterizes even the dynamics of short chains. In the present work we study also the stiffness influence in the same model, but the stiffness along the chain is implemented by other forms of the bending and torsion potential.

A different novel type of polymer model, with imposed uncrossability constraints and coarse-grain parameters derived from atomistic MD simulations (including bending stiffness), was used by Padding and Briels (2002) for linear polyethylene (PE). The onset of entanglement effects occurred at a length of $N = 6$ corresponding to a chain with 120 carbon atoms. A clear $D \propto N^{-2.2}$ was found for N between 20 and 50. The intrinsic stiffness from bending as well as torsion was also included in the atomistic MD simulation of PE performed by Harmandaris et al. (2003). Their predicted dependence of D on N has three regimes: $\nu > 1$ for $0 < N < 90$, then $\nu = 1$ for $90 < N < 156$, and $\nu = 2.4$ for $156 < N < 250$. The dependence over the first range is in agreement with Mondello et al. (1998) who suspect a sub-Rouse behavior for short chains that disobey Gaussian statistics.

Obviously, there is no consensus in the scientific literature on the scaling of the self-diffusion coefficient with chain length, nor is it clear what the value is of the entanglement length corresponding to the crossover between Rouse and reptation regimes. It is noted that the disparity is partly the result of a non-unanimous definition of N_e. Since it is a peculiar theoretical concept that cannot be measured directly, one can only see its effects on different macroscopic properties of the melt (self-diffusion, plateau modulus,

viscosity, structure factor). Inconsistent values of N_e are found based on these different properties. Furthermore, N_e depends on the level of coarse-graining used, fact that makes comparisons even more difficult.

The effect of chain stiffness on the N-dependence of D and on the value of N_e is even more complex. The available models for entanglement onset as a function of chain stiffness predict opposite behaviors, as described in an extensive review of Heymans (2000). One line of thought predicts an increase of N_e with increasing stiffness: the purely empirical equation $N_e \propto C_\infty^a$ was proposed by Aharoni (1983) with a between 0.5 and 2. Here, C_∞ is the characteristic ratio and provides a measure of chain stiffness. Wu (1989), using a topological model, introduced $a = 2$ and later Wool (1993) proposed $a = 1$. The second school of thought (Morse 1998, Fetters et al. 1999) claims that N_e decreases with increasing C_∞; this is typically expressed in terms of the packing length p_l, which is essentially C_∞^{-1} and defined as the volume occupied by a chain in the melt, divided by the mean-square chain end-to-end distance. Fetters et al. (1999) proposed $N_e \propto p_l^3$ for N_e calculated from the plateau modulus, $N_c \propto p_l^{2.35}$ for N_c from viscosity measurements and $N_r \propto p_l^{-0.9}$ for N_r — the crossover to reptation in viscosity behavior.

Against the background of the above findings, this chapter investigates the influence of chain conformational rigidity on the melt dynamics hoping to shed more insight on this still open problem. Our results indicate that the power exponents in both Rouse and reptation regimes are strongly modified by chain stiffness. Also, we find that the entanglement length increases with increasing chain rigidity. For controlling the chain stiffness we use bending and torsion potentials along the polymer chain. Our simulations employ a new torsion potential that depends on both dihedral and bending angles. This potential does not require rigid constraints on the bending angles and gracefully eliminates the computational singularities arising when two adjacent bonds align.

The chapter is organized as follows: in Sec. 4.2 we present our computational model and the potentials used to control the polymer chain rigidity. The preparation of the polymer melt and the simulation methodology are described in Sec. 4.3. Section 4.4 contains the results and the discussion of the observed static and dynamic melt properties, followed by the conclusions in Sec. 4.5.

4.2 Computational model

The system we study is an ensemble of entangled polymer chains placed in a cubic simulation box with periodic boundary conditions (see Fig. 4.1).

Each chain is modeled as a linear sequence of beads interconnected by springs, every bead representing a group of a few atoms or monomer units along the polymer backbone. The beads in the system interact via two-body potentials acting between all

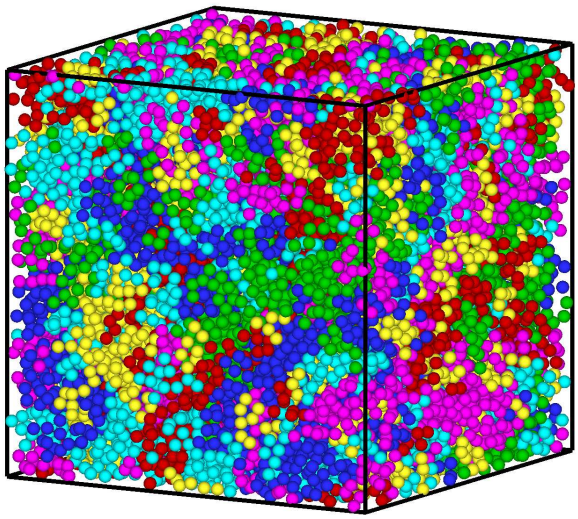

Figure 4.1: *An example of a simulation box with $M = 100$ chains each with $N = 100$ beads. All beads are represented inside the simulation box as resulting from the application of the periodic boundary conditions. Individual chains are represented in different colors.*

consecutive connected beads and between all pairs of beads in the melt. Such a model already leads to an intrinsic stiffness of the polymer chains due to the excluded volume interaction (Kremer and Grest 1990). The main goal of the study presented in this chapter is to investigate the influence of the chain stiffness on the static and dynamic properties of the polymer melt. Therefore we further enhance the chain stiffness by adding bending and torsion potentials along the chain. Depending on the actual potentials considered in the simulation, different random-walk methods are used to generate the chains close to their equilibrium configuration induced by these potentials. This will also significantly reduce the computation time needed for melt relaxation.

In the presence of bending and torsion potentials the polymer chain configuration becomes more rigid and, subsequently, more uncoiled. A classical measure used to characterize the spatial arrangement of the polymer is the *characteristic ratio* C_∞. It expresses the mean end-to-end distance of a chain with a large number of beads N (approaching ∞), separated by the average bond length b, via

$$C_\infty N b^2 = \left\langle R^2(N) \right\rangle = \left\langle |\mathbf{r}_1 - \mathbf{r}_N|^2 \right\rangle \,, \tag{4.1}$$

where $\mathbf{r}_i$ is the position vector of bead number i in the chain. The theoretical values of C_∞ are known for chains generated with specific random-walk configurations (Flory 1969) and have been introduced in Chapter 2 (Eqs. (2.5) and (2.6)). This coefficient is used as a measure of chain stiffness.

Three internal measures completely define the chain configuration: the bond length b, the bending angle θ and the dihedral angle ϕ. Based on these, we generate each

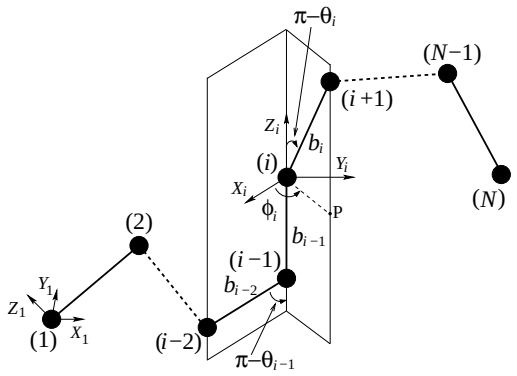

Figure 4.2: *Schematic representation of a polymer chain. Bead indices are indicated in parentheses.* b_i *is the bond length,* θ_i *is the bending angle and* ϕ_i *is the dihedral angle. The local* $(X_iY_iZ_i)$ *coordinate system is such that* Z_i *is aligned with bond* b_{i-1}*;* X_i *lies in the plane defined by bonds* b_{i-1} *and* b_{i-2} *and makes an acute angle with* X_{i-1}*;* Y_i *completes a right-handed coordinate system. P is the projection of bead* $i+1$ *on the* (X_iY_i) *plane and allows for visualization of the dihedral angle* ϕ_i*.*

polymer chain as a 3D random walk of $N-1$ steps.

Starting from bead i on the polymer chain, the next bead $i+1$ is generated by making a random move in space. In the local $(X_iY_iZ_i)$ coordinate system attached to bead i, this move is characterized by the radius b_i, the polar angle $\pi-\theta_i$ and the azimuthal angle ϕ_i (see Fig. 4.2). The local coordinates of bead $i+1$ are transformed into global Cartesian coordinates linked to the first bead by translation and rotation operations. By connecting all N beads generated in this way, we obtain a 3D random coil with $N-1$ steps or bonds. The statistical properties of such a chain (including C_∞) can be controlled by imposing specific constraints on the internal measures. We have used the following three chain generation methods:

1. Freely jointed chain (FJC): bond length b fixed, bending angle θ free in $[0°, 180°]$ and dihedral angle ϕ free in $[-180°, 180°]$. This will lead to $C_\infty = 1.0$.

2. Freely rotating chain (FRC): bond length b fixed, bending angle θ fixed to $\theta_0 = 109.5°$ and dihedral angle ϕ free in $[-180°, 180°]$. This will lead to $C_\infty = 2.0$.

3. Rotational isomeric state (RIS): bond length b fixed, bending angle θ fixed to $\theta_0 = 109.5°$ and dihedral angle ϕ constrained to three values $\phi_0 = 60°$ (gauche$^+$), $180°$ (trans) and $300°$ (gauche$^-$) with probabilities 0.2, 0.6 and 0.2 respectively. This will lead to $C_\infty = 4.7$.

In all cases we allow the parameters to vary slightly around the equilibrium values ($\pm 5\%$ for bond length and $\pm 5°$ for the angles). We impose a supplementary self-

avoiding condition to prevent subsequent Lennard-Jones instabilities. This will effectively force all bending angles to be larger than approx. 60° and will consequently lead to $C_\infty = 1.7$ instead of 1.0 for the freely jointed chains.

Let us consider further the potentials governing the interactions in the polymer melt. All beads, either belonging to the same chain or to different chains, interact via the 6-12 Lennard-Jones (LJ) potential, cut off at its minimum ($r_{\mathrm{cut-off}} = \sqrt[6]{2}\sigma$) and shifted such that it vanishes at $r_{\mathrm{cut-off}}$ (Weeks et al. 1971):

$$V_{\mathrm{LJ}}(r_{ij}) = 4\varepsilon \left[\left(\frac{\sigma}{r_{ij}} \right)^{12} - \left(\frac{\sigma}{r_{ij}} \right)^{6} + \frac{1}{4} \right], r_{ij} < r_{\mathrm{cut-off}}, \tag{4.2}$$

where $r_{ij} = |\mathbf{r}_i - \mathbf{r}_j|$ is the distance between beads i and j. The Lennard-Jones parameters ε and σ are the characteristic energy and length scales. The time unit becomes $\tau = \sigma(m/\varepsilon)^{1/2}$, where m is bead mass. We run our MD simulations and report most of our results using reduced units, i.e. $\sigma = 1$, $\varepsilon = 1$, $m = 1$ and Boltzmann's constant $k_B = 1$.

In addition to the Lennard-Jones interaction, adjacent bonded beads interact by an attractive Finite Extensible Non-Linear Elastic (FENE) potential:

$$V_{\mathrm{FENE}}(r_{ij}) = \begin{cases} -0.5kR_0^2 \ln\left[1 - (r_{ij}/R_0)^2\right], & r_{ij} \leq R_0 \\ \infty, & r_{ij} > R_0 . \end{cases} \tag{4.3}$$

The spring constant k is chosen as $k = 30\varepsilon/\sigma^2$ while we take $R_0 = 1.5\sigma$ for the maximum bond extension. Superposition of the LJ and FENE potentials, with these specific parameter values, yields an anharmonic spring interaction between connected beads with equilibrium bond length $b = 0.96\sigma$. During simulations at $T = 1.0\varepsilon/k_{\mathrm{B}}$, the bond length will always be less than 1.2σ. As a consequence, bond crossing is energetically unfavorable and chain entanglement is naturally obtained (Kremer and Grest 1990).

Supplementary to these two interactions, we consider first bending and then combined bending and torsion potentials to enhance the polymer rigidity.

The stiffness of FRC and RIS generated chains is controlled by a bending potential, which acts on three consecutive beads along the chain. The angle between adjacent pairs of bonds is maintained close to the equilibrium value $\theta_0 = 109.5^\circ$ by the cosine harmonic bending potential

$$V_{\mathrm{B}}(\theta_i) = \frac{1}{2} k_\theta (\cos\theta_i - \cos\theta_0)^2, \tag{4.4}$$

where θ_i is the bending angle between bonds b_{i-1} and b_i. The value of the bending constant k_θ is varied to obtain different chain stiffness with the corresponding characteristic ratios.

For RIS generated chains, in addition, a torsion potential acting on four consecutive beads is employed. This potential mainly constrains the dihedral angle ϕ_i, which is

defined by three successive bonds, b_{i-2}, b_{i-1} and b_i. We propose here a novel form for the torsion potential:

$$V_{\mathrm{T}}(\theta_{i-1}, \theta_i, \phi_i) = k_\phi \sin^3\theta_{i-1} \sin^3\theta_i \sum_{n=0}^{3} a_n \cos^n\phi_i. \tag{4.5}$$

This potential not only depends on the dihedral angle ϕ_i but also on the bending angles θ_{i-1} and θ_i formed by the three successive bonds. The third-order polynomial in $\cos\phi_i$ follows from *ab initio* calculations for n-butane (Steele 1985) and has coefficients $a_0 = 3.00$, $a_1 = -5.90$, $a_2 = 2.06$, $a_3 = 10.95$. It has three minima for $\phi = 180°$ (trans), $\phi = 60°$ (gauche$^+$) and $\phi = 300°$ (gauche$^-$). The two $\sin^3\theta$ pre-factors, tentatively suggested by Scott and Scheraga (1966), cancel the torsion potential and force when either of the two bending angles vanishes, which would make the dihedral angle ϕ undefined. This important property makes the potential well-behaved for MD simulations that have no rigid constraints on the bending angles; torsion potentials that are independent of the bending angles suffer from the problem that the torsion forces tend to infinity when two consecutive bonds are aligned. A strong bending potential may prevent this tendency, but when bonds align the simulation breaks down. The torsion potential proposed here gracefully eliminates these singularities and leads to stable MD runs. The value of the torsion constant k_ϕ was varied for stiffness control.

It is important to note that the bending and torsion potentials together form a combined potential $V_{\mathrm{CBT}} = V_{\mathrm{B}} + V_{\mathrm{T}}$ that determines the dynamics of the polymer chain. V_{CBT} induces a new equilibrium bending angle θ_{eq} that is slightly larger than θ_0 resulting from V_{B} only, while the equilibrium torsion angles are identical with those induced by V_{T}. The average bond length is unaffected by including stiffness along the chain.

4.3 Sample preparation

The polymer melt samples are prepared in three steps:

1. First, we generate an ensemble of individual polymer chains, using one of the three chain generation methods discussed above.

2. These chains are placed together inside the simulation box using a packing procedure that minimizes the variation of the local bead density.

3. The bead overlaps are eliminated in a pre-equilibration MD run that uses a threshold LJ interaction.

The simulated system is a cubic box containing a total of M chains with N beads per chain, at a bead number density $\rho = 0.85\sigma^{-3}$ as in (Kremer and Grest 1990). The

simulation box is filled by placing the M chains with their centers of mass in randomly distributed points inside the box. As a result, the local bead density is not uniform throughout the simulation box. In order to homogenize it, an MC-like algorithm is employed that minimizes the variance of the local bead density. Our packing method is a simplification of the method discussed by Auhl et al. (2003). The MC 'moves' are small geometric transformations that act separately on a polymer chain: translation, rotation or reflection. During these transformations, the chains are treated as rigid objects, their internal spatial configuration remaining unaffected. One transformation randomly chosen from the repertoire of three is applied to a randomly chosen chain. All 'moves' that increase the variance of local bead density are rejected and only those that decrease it are accepted until a desired homogeneity is reached.

After this packing process, there will be many bead overlaps and switching on the LJ potential would inevitably lead to numerical instabilities. In order to avoid this, a temporary MD simulation is performed using a modified LJ potential: the LJ force between two particles that are closer than a threshold distance $d = 1.0\sigma$ is replaced with the LJ force at this distance. The particles that are a 'safe' distance apart are subjected to the full LJ force. In order to allow the beads to move apart easier, the bending and torsion potentials are turned off during this pre-equilibration stage. The modified MD simulation is performed with this threshold LJ force until all beads are pushed away from the overlap regions. Then, the full LJ, bending and torsion potentials are turned-on and the main MD simulation can start. This technique for eliminating the bead overlaps, a simplification of the "slow push off" method of Auhl et al. (2003), guarantees a small perturbation of the chain configurations at the transition from modified to full LJ potential.

We perform a series of MD runs at constant temperature T and volume V (NVT equilibrium simulations). The equations of motion are integrated using the 'velocity-Verlet' algorithm (Swope et al. 1982) with a time step $\Delta t = 0.01\tau$. The temperature is kept constant by coupling the system to a heat bath: the friction coefficient is $\Gamma = 0.5\tau^{-1}$ and the strength of the Gaussian white-noise force is $6k_BT\Gamma$ (Grest and Kremer 1986). Due to the random force, the center of mass of the entire system will drift. We remove this drift for the subsequent analysis of the chain motion. Results will be present for systems with up to $M = 1000$ chains, for chain lengths between $N = 5$ and $N = 250$. One of the longest simulated times was $2 \times 10^5\tau$.

Fig. 4.3 represents the flow-chart of our MD code used for the simulation of a polymer melt.

Our code has an average speed of 1.9×10^5 particle updates per second on a 2.8 GHz / 1 GB Pentium 4 processor. The results reported in this chapter are based on a total computation time of approximately 4 CPU years.

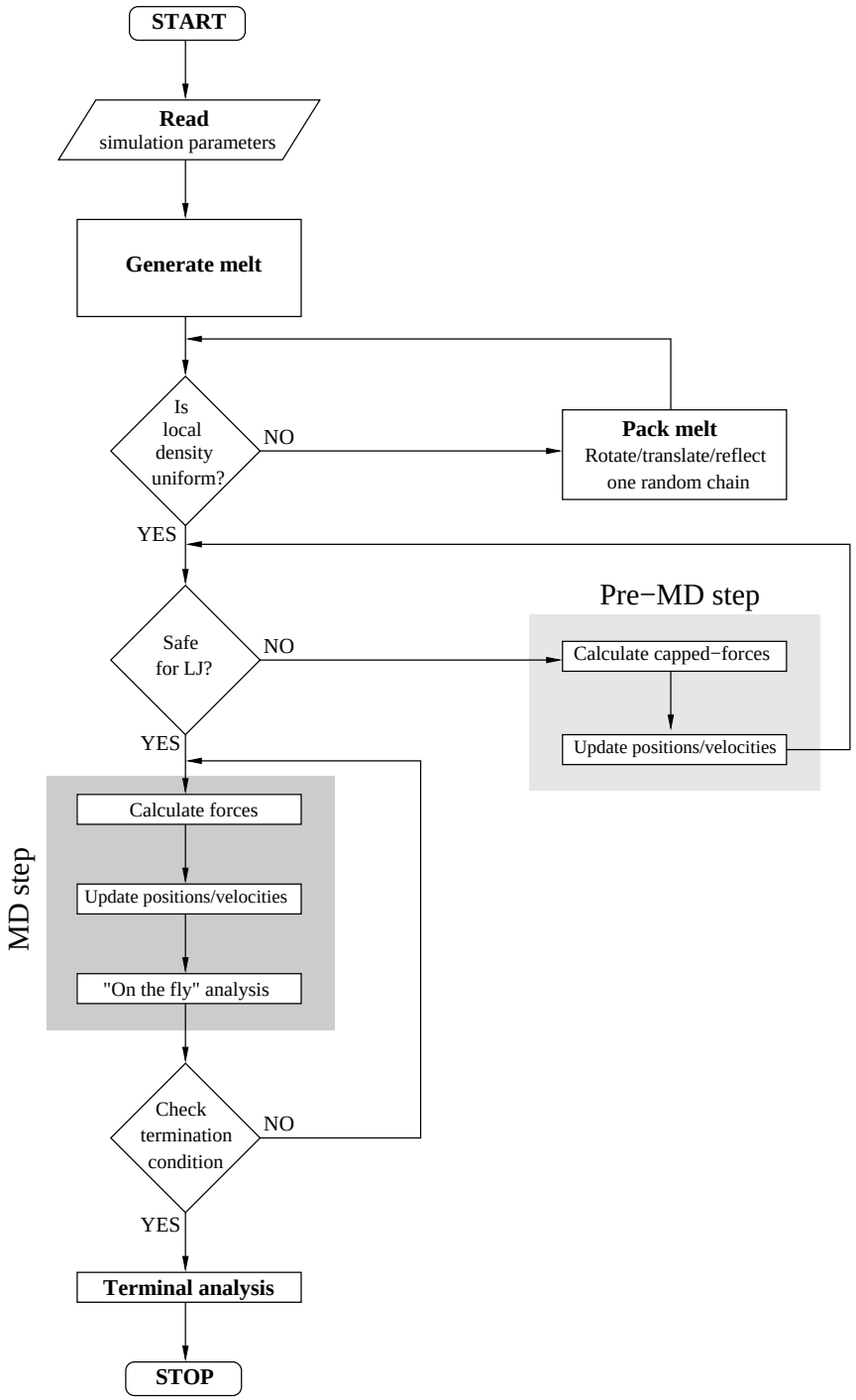

Figure 4.3: *Schematic representation of the program used for simulations of the polymer melt.*

4.4 Results and discussion

The objective of this study is to find out how an increasing chain stiffness affects the properties of the entangled polymer melt. In order to characterize in detail the melt behavior we investigate both its static and dynamic properties.

4.4.1 Static properties

A natural way to characterize polymer melts after equilibration is the N-dependence of the mean-square end-to-end distance $\langle R^2 \rangle$ and radius of gyration $\langle R_g^2 \rangle$ averaged over all chains in the melt. In order to increase the statistical ensemble of R^2 and R_g^2, we compute them not only for the entire chains, but also for all their sub-chains. Flory's theory (Flory 1969) predicts that the chains of the equilibrated melt obey Gaussian statistics with: $\sqrt{\langle R^2 \rangle} \propto N^{0.5}$, $\sqrt{\langle R_g^2 \rangle} \propto N^{0.5}$ and $\langle R^2 \rangle / \langle R_g^2 \rangle = 6$. Our numerical results, collected in Table 4.1, are generally consistent with these theoretical predictions. However, some numerical deviations can be observed, especially for the ratio $\langle R^2 \rangle / \langle R_g^2 \rangle$ which exceed the value 6.0 when the chain stiffness is increased. The measured values for C_∞ increase with increasing stiffness, in general agreement with the theoretical principles. Figure 4.4 shows the N-dependence of $\langle R^2 \rangle$ and $\langle R_g^2 \rangle$ for few selected cases from Table 4.1.

k_θ (ε)	k_ϕ (ε)	t ($\tau \times 10^5$)	α	β	$\langle R^2 \rangle / \langle R_g^2 \rangle$	C_∞
0	0	2	0.52	0.52	5.99	1.69
25	0	1	0.53	0.54	5.97	1.94
35	0	2	0.54	0.54	6.23	2.24
50	0	2	0.55	0.54	6.24	2.33
100	0	1.5	0.55	0.54	6.26	2.42
25	0.2	2	0.57	0.57	6.43	3.30
25	0.5	2	0.57	0.58	6.41	4.00
25	1	2	0.61	0.62	6.68	5.81

Table 4.1: *Static properties of systems with $M = 100$ chains and $N = 200$ beads at a temperature $T = 1.0\varepsilon/k_B$, for different values of the bending (k_θ) and torsion (k_ϕ) constants. t is the total simulation time, α is the exponent in $\sqrt{\langle R^2 \rangle} \propto N^\alpha$, β is the exponent in $\sqrt{\langle R_g^2 \rangle} \propto N^\beta$, and C_∞ is the characteristic ratio defined in Eq. (4.1).*

Important information about static properties can be extracted from the distributions of bond lengths, bending and torsion angles after equilibration. Their profiles give direct evidence for the action of considered potentials.

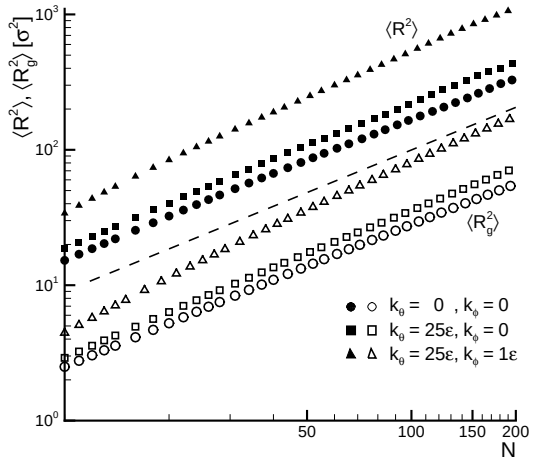

Figure 4.4: *Mean-square internal end-to-end distance $\langle R^2(N)\rangle$ (black symbols) and radius of gyration $\langle R_g^2(N)\rangle$ (open symbols) vs. N for melts with $M = 100$ chains of length $N = 200$ beads for different chain flexibilities k_θ and k_ϕ. The dashed line is a visual aid representing the theoretical scaling $\propto N^{0.5}$.*

The histogram of bond lengths, presented in Fig. 4.5a, reveals the slight asymmetry around the equilibrium bond, induced by the LJ and FENE potentials considered between consecutive beads. The angle potentials are reflected both in the histograms of bending and torsion angles. As can be seen in Fig. 4.5b, the increase of bending stiffness leads to higher and narrower peaks about the equilibrium angle in the bending histogram. In Fig. 4.5c the effect of the torsion potential on the dihedral angle distribution is illustrated: three maxima appear for the gauche$^-$, trans and gauche$^+$ states. When the torsion constant k_ϕ is increased, only the trans maximum is significantly modified and, as a result, the ratio between the trans/gauche states increases.

At this point, we recall that the bending (Eq. (4.4)) and torsion (Eq. (4.5)) potentials have to be considered together in a combined bending-torsion form (CBT) because their effects on the polymer dynamics cannot be separated. For a case in which the bending constant is $k_\theta = 25\varepsilon$, two effects can be observed in the bending histogram when we add a torsion potential with $k_\phi = 3\varepsilon$: a broadening towards larger θ-angles and a slight shift of the equilibrium angle $\theta_{\rm eq} > \theta_0$ (see Fig. 4.5b). Complementary, if the torsion strength is kept constant at $k_\phi = 1\varepsilon$, an increase of the bending constant from $k_\theta = 25\varepsilon$ to $k_\theta = 100\varepsilon$ leads to a sharper peak for the trans state (see Fig. 4.5c). This effect is attributed to the fact that as the bending potential gets stronger, the bonds are not allowed to straighten and, as a consequence, the torsion potential is effectively stronger. The examples provided in Fig. 4.5 are rather extreme cases that serve illustrative purposes; in most subsequent simulations we use values for the bending and torsion constants which induce only moderate deviations in the angular distributions.

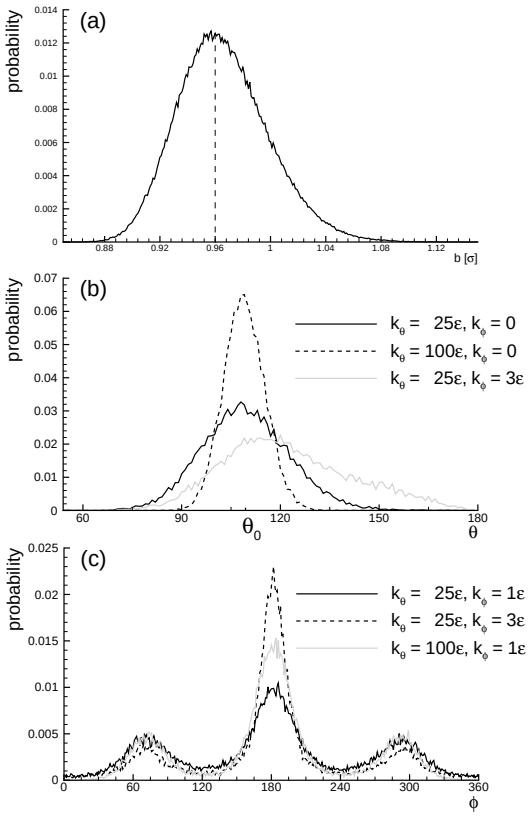

Figure 4.5: *Histograms of bond lengths (a), bending angles (b) and torsion angles (c) after equilibration of $M = 100$, $N = 40$ systems for $t = 10^5\tau$. The equilibrium bond is $b = 0.96\sigma$ and the equilibrium bending angle is $\theta_0 = 109.5°$. The histograms are the average result over 10 distributions.*

During melt relaxation, a local structure appears naturally in the system, which can be illustrated by the pair distance correlation function $g(r)$, shown in Fig. 4.6, plotting the correlation for the intra and inter-chain beads separately. The intra $g(r)$ has a sharp peak at $r \approx \sigma$, corresponding to the connected beads and the inter $g(r)$ has two expected peaks due to the first two LJ spheres of influence. The stiffness effects are evident in the intra-chain pair distance correlation: the bending potential introduces an intermediate peak at $r = 2b\sin(\theta_0/2) \approx 1.6\sigma$, corresponding to all the bead-pairs (i, $i+2$) and some of the (i, $i+3$) pairs. The remaining (i, $i+3$) pairs form a weak peak at $\approx 2.5\sigma$. The introduction of torsion stiffness has the effect of uncoiling even more the polymer chain with direct result in decreasing the first intra-chain peak (an effect already observed in the bending histograms) and in increasing the second one.

Another straightforward way to analyze the equilibrated melt is to analyze the chain

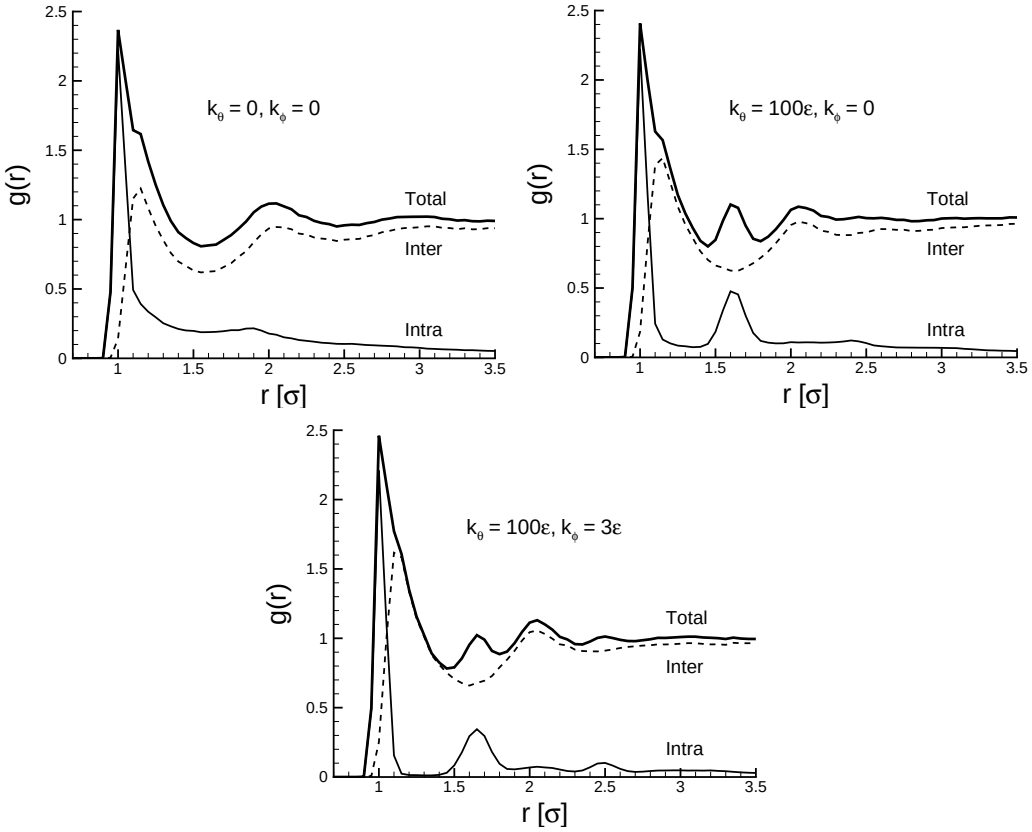

Figure 4.6: *Pair distance correlation function $g(r)$ (for intra-chain, inter-chain and all beads) for different stiffness in melts with $M = 1000$, $N = 40$.*

Rouse modes. For each time these are given by:

$$\mathbf{X}_p(t) = \frac{1}{N}\sum_{j=1}^{N} \mathbf{r}_j(t) \cos\left[\frac{p\pi}{N}\left(j - \frac{1}{2}\right)\right], \tag{4.6}$$

where $p = 0, 1, ...N-1$ is the mode number, describing a wavelength corresponding to a sub-chain of $N/(p+1)$ beads. Even though we do not expect the Rouse modes to be exact eigenmodes for entangled polymer chains with included stiffness, we still investigate their static autocorrelation as a function of p and compare it with the scaling relations proposed in the Rouse model:

$$\langle \mathbf{X}_p(0) \cdot \mathbf{X}_p(0) \rangle = \frac{l^2}{2N\lambda_p}\,; \lambda_p = 4\sin^2\left(\frac{p\pi}{2N}\right). \tag{4.7}$$

In addition, we compare the results with the analytical expression

$$\langle \mathbf{X}_p(0) \cdot \mathbf{X}_p(0) \rangle = \frac{l^2}{2N}\left[\frac{1}{\lambda_p} - \frac{1}{\gamma^2 + \lambda_p}\left(1 + O(N^{-1})\right)\right] \tag{4.8}$$

with

$$\gamma^2 = \frac{1 - |\langle \cos\theta \rangle|^2}{4\,|\langle \cos\theta \rangle|} \tag{4.9}$$

for FRC chains with a specific bending angle θ (Kreer et al. 2001). In the limit of large N, Eq. (4.7) gives the well-known dependence as p^{-2} of the modes autocorrelation, while Eq. (4.8) provides a p^{-3} dependence, already observed for large modes (Krushev et al. 2002).

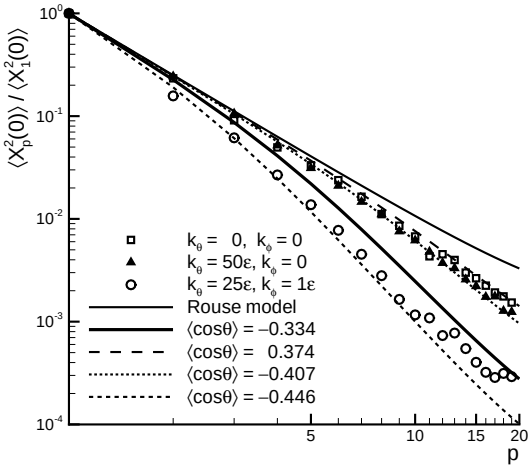

Figure 4.7: *Normal mode amplitudes (normalized by the first mode) vs. mode number p for melts with $N = 35$ beads and different stiffness. The solid thin line represents the Rouse prediction (Eq. (4.7)) and the other lines correspond to the FRC model with different values of $\langle \cos\theta \rangle$ (Eq. (4.8)).*

Figure 4.7 presents the results for the first 20 modes for systems with $N = 35$ beads, with different stiffness. For the fully flexible chains, the Gaussian p^{-2} dependence is recovered (fit: $p = 2.1$) but the deviations between the simulation results and the exact Rouse prediction (Eq.(4.7)) gradually develop with increasing the mode number.

This is to be expected since p/N is relatively large and the intrinsic stiffness from excluded volume, present at the local scale, cannot be ignored. If this stiffness is characterized by an average bending angle in Eq. (4.8) the best fit is obtained for $\theta \approx 68°$.

When the stiffness is increased the deviation from the pure Rouse model becomes more evident. The overall p-dependence becomes $p^{-2.3}$ and $p^{-2.6}$ for bending (triangles) and for bending plus torsion (circles). The best fit with the FRC model prediction indicates $\theta \approx 114°$ for bending and $\theta \approx 116.5°$ for bending plus torsion. Thus, additional stiffness modifies the dependence of the normal mode amplitude on p, while the torsion effects are clearly separated from the bending effects.

4.4.2 Dynamic properties

The motion of polymer chains in the melt can be suitably analyzed by monitoring how the beads and the chain centers of mass diffuse in time. The self-diffusion coefficient, characterizing the macroscopic transport of the chains inside the polymer melt, is calculated from the mean-square displacement using the Einstein relation.

Specifically, in order to characterize the melt dynamics, three mean-square displacements are computed during the MD simulation: the absolute bead mean-square displacement $g_1(t)$ (Eq. (2.9)), the bead mean-square displacement relative to the chain's center of mass $g_2(t)$ (Eq. (2.10)) and the mean-square displacement of the chain center of mass $g_3(t)$ (Eq. (2.11)).

The center of mass of the whole melt is held fixed at the origin to eliminate its drift due to the stochastic force modeling the thermostat. The mean values of $g_1(t)$, $g_2(t)$ and $g_3(t)$ are computed by averaging over all chains in the melt. An important aspect is that we only consider the central part of the chains (the five most internal beads) for computing the bead mean-square displacements $g_1(t)$ and $g_2(t)$. This ensures that we only account for the central beads of a chain which fully experience the effects of the chain entanglement and not the chain ends which have a more freely exploring motion.

The self-diffusion coefficient D of the chains inside the polymer melt is computed from the slope of $g_3(t)$ using the Einstein relation

$$D = \lim_{t\to\infty} \frac{1}{6t} g_3(t)\,. \tag{4.10}$$

According to the Rouse model, the diffusion coefficient is expected to reach the asymptotic value

$$D = \frac{k_B T}{\zeta N} \tag{4.11}$$

for relatively short times, ζ being the effective bead friction coefficient. For long entangled chains, reptation theory predicts a different coefficient, corresponding to the drastic slow down of the chain motion:

$$D = \frac{1}{3}\frac{d_{\mathrm{T}}^2}{l^2}\frac{k_B T}{\zeta N^2}\,, \tag{4.12}$$

where d_{T} is the tube diameter and l ($l^2 = C_\infty b^2$) is the effective bond length.

A proper value for D can only be obtained if the chains diffuse more than their radius of gyration. We have ensured that the computing times were long enough for this condition to be met even for the longest stiff chains.

First we investigate how diffusion is affected by the chain rigidity for a melt with $M = 100$ chains of length $N = 40$. The dependence of the self-diffusion coefficient D on the bending and torsion strengths is displayed in Fig. 4.8. A power-law fit of this

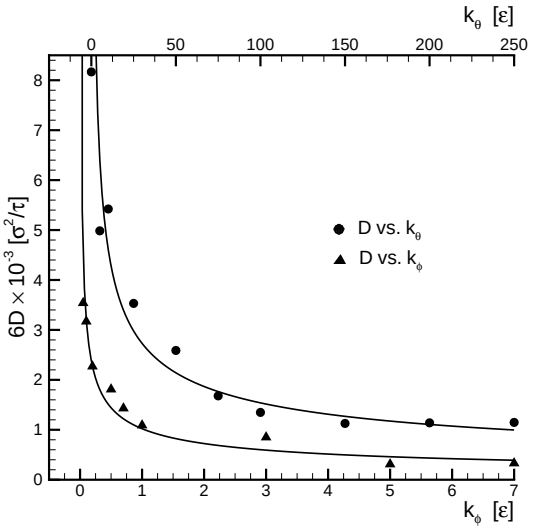

Figure 4.8: *D vs. k_θ and vs. k_ϕ for a melt with $M = 100$ chains, $N = 40$ beads per chain.*

data yields $D \propto k_\theta^{-0.48}$ and $D \propto k_\phi^{-0.54}$, which indicate a high sensitivity of diffusion to the bending (three-body) and torsion (four-body) interactions. The eigen-frequencies of the bending and torsional vibrations in a chain are proportional to the square root of the spring constants k_θ and k_ϕ. Thus, we conclude that the self-diffusion coefficient D is inversely proportional to the eigen-frequencies of the angular vibrations about the polymer backbone.

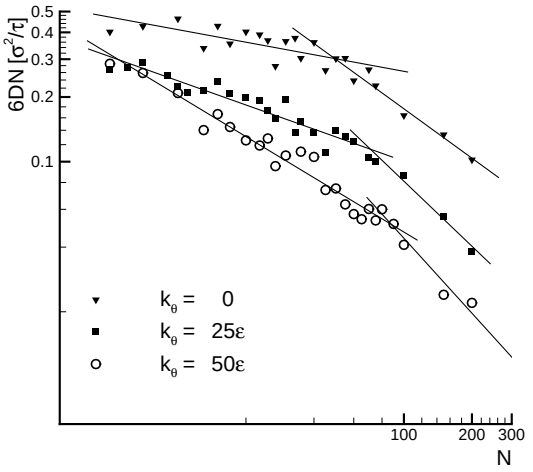

Figure 4.9: *The dependence of $6DN$ on N for different bending rigidities in the absence of torsion stiffness, $k_\phi = 0$.*

Figure 4.9 reports the computed values of $6DN$ as a function of N (on log-log scales)

for different chain rigidities controlled by the bending potential, at the same temperature $T = 1.0\varepsilon/k_B$. The product $6DN$ is chosen to emphasize the different regimes in $D(N)$ as will become clear further on. For all cases presented in the figure, two distinct diffusion regimes can be identified with the naked eye. A more objective separation between these was obtained by maximizing the sum of regression coefficients of two consecutive lines fitting the data, with slopes close to 1 and 2. The results –slopes ν_1, ν_2 for the two regimes and the crossover between them, N_e– are shown in Table 4.2.

k_θ (ε)	k_ϕ (ε)	N_e	ν_1	ν_2	ζ (τ^{-1})
0	0	≈ 70	1.1	1.7	25
25	0	≈ 75	1.4	2.2	80
50	0	≈ 80	1.6	2.1	92
25	0.5	≈ 90	1.7	2.2	290
25	1	–	1.9	–	806

Table 4.2: *The influence of chain rigidity on the values of N_e, exponents ν_1 and ν_2 in the power-law $D \propto N^{-\nu_i}$ and ζ the bead friction coefficient for the two distinct diffusion regimes.*

To test this 'automatic crossover detector', we have applied it to the diffusion data from the established work of Kremer and Grest (1990), and the crossover between Rouse regime and reptation regime was found at $N_\mathrm{e} \approx 40$ as expected. For the case with chain stiffness resulting only from the excluded volume interactions, our data (with more simulated points for the $6DN$ vs. N dependence) indicate $N_\mathrm{e} \approx 70$, which is in excellent agreement with that reported by Pütz et al. (2000).

In Fig. 4.10 we present $D(N)$ results for chain rigidities induced by the torsion potential, keeping the bending strength constant at $k_\theta = 25\varepsilon$, a medium-high value used in Fig. 4.9.

The effect of torsion stiffness is similar in qualitative terms to what we have found for bending. But, torsion appears to have a much stronger effect on chain dynamics. The diffusion results with a low value of the torsion constant ($k_\theta = 25\varepsilon$, $k_\phi = 1\varepsilon$) nearly overlap with those for a very strong bending potential acting alone ($k_\theta = 100\varepsilon$) (data not shown). When both bending and torsion potentials are used, all degrees of freedom of the polymer chain tend to be constrained during the dynamics, thus having a significant influence on the resulting macroscopic transport properties. This observation is consistent with recent studies highlighting the central importance of torsion dynamics in polymer relaxation processes (Paul and Smith 2004).

From Figure 4.9 and Fig. 4.10 four effects are observed when the bending and torsion chain rigidity is increased:

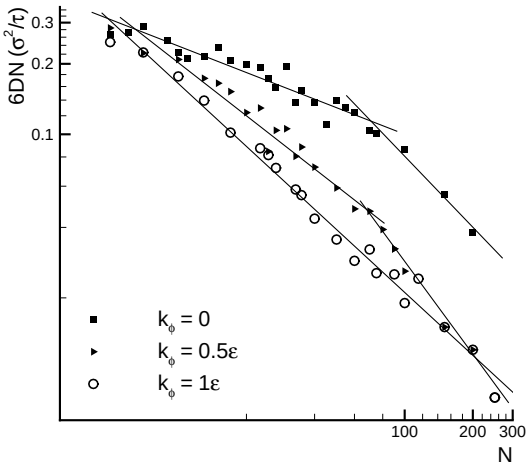

Figure 4.10: *The dependence $6DN$ vs. N for different torsion rigidities, at a constant bending strength $k_\theta = 25\varepsilon$.*

- the self-diffusion coefficient decreases for all chain lengths;
- in the regime of shorter chains the diffusion dependence on N becomes steeper; nevertheless, we will continue to name it "Rouse regime" because it is followed by an even steeper dependence corresponding to reptation;
- the crossover between the (modified) Rouse and reptation regimes moves to longer chains, until it becomes undefined when the slopes of the two regimes can no longer be distinguished.
- the slope ν_2 characteristic in the reptation regime increases to the value $\nu_2 = 2.2$ (see Table 4.2), in agreement with recent theoretical, experimental and computational work (Frischknecht and Milner 2000, Lodge 1999, Tao et al. 2000, Padding and Briels 2002).

The dramatic decrease of D is reflected in an increase of the bead friction coefficient ζ with increasing chain stiffness (Table 4.2 includes the computed values of ζ from the bead mean-square displacement, analyzed in next sub-section).

The modification of the Rouse regime (ν_1 becoming larger than unity) has already been noticed in earlier numerical and experimental work. Some authors (Pearson et al. 1994) assume that the Rouse prediction for the self-diffusion vs. N is accurate and correct the experimental data by allowing for a dependence of the bead friction coefficient on the chain length. However, care should be taken of the fact that the density in experiments fluctuates with the chain lengths, while in our simulation it is kept constant. Another important factor is the influence of the glass transition on friction; future computer simulations at the same T/T_g have to be performed.

The temperature effects are evident in pulsed-gradient spin-echo NMR measurements of D for n-alkanes (von Meerwall et al. 1998) in which an exponent $\nu_1 \neq 1$ has been observed below the onset of entanglement. The experimentally obtained exponent changes monotonically from 1.85 to 2.72 as T decreases from $443K$ to $303K$, suggesting the existence of free-volume effects on self-diffusion. By increasing the chain stiffness and consequently limiting the freedom of chain ends, we obtain the same trends for the power exponent as in the experimental work on decreasing temperature. Atomistic MD simulations, at constant pressure, (Harmandaris et al. 2003) have also shown a modification of the Rouse regime that was explained by free-volume effects.

In a united-atom MD simulation of melts of short n-alkanes, Mondello et al. (1998) found a "sub-Rouse regime" with a power exponent ν_1 between 1 and 2. This behavior was explained by the deviation of short chains from exact Gaussian statistics. To a certain extent, such a deviation is also observed in our results as we increase the chain stiffness, see Table 4.1. The Rouse and reptation theories assume Gaussian chains and this disparity can be one of the origins for the deviation between computational and theoretical predictions.

In summary, the unknown dependence of friction coefficient on N, the deviation from Gaussian statistics as well as the free-volume effects seem possible explanations for the modification of the Rouse regime when stiffness is added to the system.

The N_{e} values presented in Table 4.2 are obtained from the $6DN$ vs. N dependence and correspond to the approximate chain length at which the crossover between Rouse and reptation regimes appears. Even though these values, as well as C_∞ cannot be established with great accuracy, one does note the tendency that N_{e} slightly increases as the chain bending rigidity increases. A clear dependence law is almost impossible to be obtained but, from all the empirical and theoretical predictions, Aharoni's equation (Aharoni 1983) ($N_{\mathrm{e}} \propto C_\infty^a$) with $a < 1$ is the most likely for our data.

This outcome seems to be in contrast with similar MD studies investigating the bending influence on melt dynamics (Faller and Müller-Plathe 2001, Everaers et al. 2004), which conclude that N_{e} decreases with chain stiffness. The reason for this apparent contradiction resides in subtle implementation differences, pertaining to the exact form of the bending potential and the value of the equilibrium angle used. Their chains are generated through non-reversal random walk, and during the MD simulation the equilibrium bending angle is kept to 180° with a relatively small energy cost. In contrast, we generate the chain as FRC (RIS) and the equilibrium bending angle is strongly kept at this value. As a result, the persistence lengths in the two simulations are almost the same but they characterize very different chain rigidities and bead friction coefficients. Thus, it not impossible that the final predictions for N_{e} in such dissimilar systems to differ.

A key intriguing question arises from the dependence of D on N for increasing chain

rigidity: what is the exact nature of the modified Rouse regime? What kind of motion does the polymer chain undertake inside the melt for this regime? In an attempt to clarify this, we further study the time dependence of mean-square displacement of a single bead from the chain, g_1.

The theoretically expected behavior of $g_1(t)$ in the Rouse and reptation models is different.

- In the Rouse model, $g_1(t)$ has two visible regimes (de Gennes 1967):

$$g_1(t) = \begin{cases} 2l^2\sqrt{\frac{W}{\pi}}t^{1/2} & \text{for} \quad \tau_0 < t < \tau_\mathrm{R} \\ 6D_0 t & \text{for} \qquad t > \tau_\mathrm{R} \end{cases} \tag{4.13}$$

  where l is the effective bond length, $W = 3k_BT/(\zeta l^2)$ the characteristic Rouse frequency, and D_0 the bead diffusion coefficient. The crossover between these two regimes occurs at the Rouse time

$$\tau_\mathrm{R} = \frac{\zeta N^2 l^2}{3\pi^2 k_B T}, \tag{4.14}$$

  i.e. the time needed for a chain with N beads to diffuse a distance equal to its mean radius of gyration, $g_1(\tau_\mathrm{R}) \approx \left\langle R_\mathrm{g}^2(N)\right\rangle$.

- In the reptation model $g_1(t)$ has an extra, weaker time dependence $g_1(t) \propto t^{1/4}$ embedded inside the $t^{1/2}$ regime:

$$g_1(t) = \begin{cases} 2l^2\sqrt{\frac{W}{\pi}}t^{1/2} & \text{for} \quad \tau_0 < t < \tau_\mathrm{e} \\ \sqrt{\frac{2}{3}}ld_\mathrm{T}\sqrt[4]{\frac{W}{\pi}}t^{1/4} & \text{for} \quad \tau_\mathrm{e} < t < \tau_\mathrm{R} \\ \sqrt{\frac{2}{N}}ld_\mathrm{T}\sqrt{\frac{W}{\pi}}t^{1/2} & \text{for} \quad \tau_\mathrm{R} < t < \tau_\mathrm{d} \\ \frac{2}{N^2}d_\mathrm{T}^2\frac{W}{\pi}t & \text{for} \qquad t > \tau_\mathrm{d} \end{cases} \tag{4.15}$$

  where d_T is the effective tube diameter. The pre-factors used in the $g_1(t)$ dependence are the same as used by Pütz et al. (2000) to enable a clear comparison. The $t^{1/4}$ regime in Eq. (4.15) is usually considered as the reptation "fingerprint". Between the entanglement time $\tau_\mathrm{e} \approx \tau_\mathrm{R}(N_\mathrm{e})$ and the Rouse time τ_R, the chain moves like a Rouse chain "trapped" inside a tube that materializes the constraints induced by the entanglements. The tube diameter is related to the radius of gyration of a chain with N_e beads through the relation $d_\mathrm{T}^2 \approx \langle R_\mathrm{g}^2(N_\mathrm{e})\rangle$. After τ_R the chain acts like a free Rouse chain with the usual $t^{1/2}$ and t^1 regimes and the crossover at the disentanglement time τ_d.

We are interested in finding out which of the two models fits best with our MD simulation results for $g_1(t)$ computed for inner beads. To analyze the character of the modified Rouse regime found in the $D(N)$ dependence, we have computed $g_1(t)$ for melts with short chains of length $N = 35$, see Fig. 4.11. As expected, when the chain stiffness increases, the diffusion of the central beads decreases. We observe that, for all cases of chain stiffness considered, $g_1(t)$ has only two power-law regimes, which are qualitatively consistent with the predictions of the Rouse model. Small deviations from the theoretical values of the exponents are observed but this is consistent with other results from MC studies of polymer melts (Paul 2002). The value of $g_1(\tau_{\rm R})$, at the crossover between the two regimes, slightly increases with increasing chain stiffness. This is consistent with the small increase in the scaling behavior of $\langle R_{\rm g}^2 \rangle$ with increasing chain stiffness according to Table 4.1.

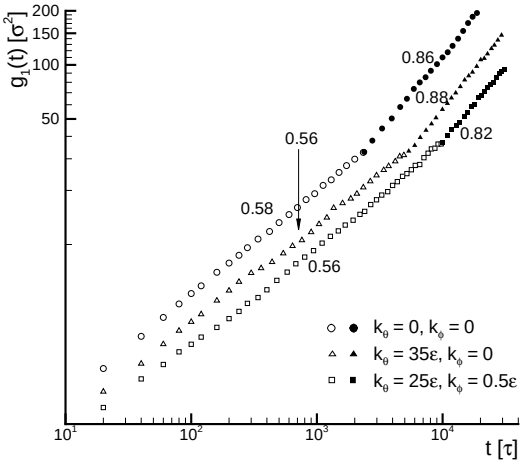

Figure 4.11: *Mean-square displacement of the innermost beads, g_1 vs. time, for a melt with $M = 1000$ chains, $N = 35$ beads per chain. The numbers are the approximate power-law exponents in $g_1 \propto t^{\alpha}$ inferred from the data points. For clarity, the symbol colors also reflect the exponents: open symbols for $\alpha \approx 1/2$ and black symbols for $\alpha \approx 1$.*

To study the effects of chain rigidity on the entanglement length $N_{\rm e}$, we have also computed $g_1(t)$ for melts with long chains ($N = 200$), see Fig. 4.12. When the bending and torsion potentials are not included (circles in the figure), $g_1(t)$ exhibits four regimes consistent with the reptation theory, even though the exponents deviate somewhat from those in Eq. (4.15). So, the FJC results confirm the known reptation motion of long polymers in melts (Kremer and Grest 1990, Pütz et al. 2000). By increasing the chain rigidity, the reptation character of the chain motion remains essentially unchanged, albeit with some subtle differences. For instance, the power exponent corresponding to the "fingerprint" reptation regime, while larger than expected, decreases towards the $1/4$ value with increasing stiffness. The same tendency was observed for increasing chain

length in other coarse-grained MD simulations (Pütz et al. 2000). Also we notice that the crossover points between all regimes are shifted to longer times and diffusion distances as the stiffness is increased.

Nevertheless, the most significant for this study is the first crossover between the $t^{1/2}$ and $t^{1/4}$ regimes. From this, we approximate the $\tau_{\rm e}$ for the cases presented in Fig. 4.12: 1000τ, 6000τ and $60,000\tau$ with increasing stiffness. The corresponding friction coefficient ζ has also been computed from the slope of g_1 vs. $t^{1/2}$ for the first regime: $\zeta \approx 25\tau^{-1}$, $\approx 85\tau^{-1}$ and $\approx 290\tau^{-1}$, respectively. Combining these results in Eq. (4.14) that, for $N = N_{\rm e}$, gives the value of $\tau_{\rm e}$, we can evaluate the $N_{\rm e}$ to be: 27, 32 and 42, respectively. These are about half of the predicted values from the diffusion analysis (fact already known in the literature) (Kremer and Grest 1990, Pütz et al. 2000) and show the same increasing tendency with increasing stiffness.

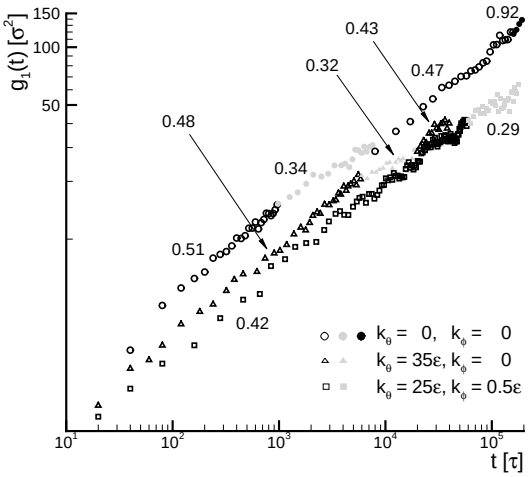

Figure 4.12: *Mean-square displacement of the innermost beads g_1 vs. time for a melt with $M = 100$ chains, $N = 200$ beads per chain. The numbers are the approximate power-law exponents in $g_1 \propto t^{\alpha}$ inferred from the data points. For clarity, the symbol colors also reflect the exponents: open symbols for $\alpha \approx 1/2$, gray symbols for $\alpha \approx 1/4$ and black symbols for $\alpha \approx 1$.*

Next, in order to characterize the motion of the chain sub-units, with different lengths, we investigate the time dependence of the normalized Rouse mode autocorrelation functions. Within the Rouse model each of the modes relaxes independently and exponentially with a relaxation time τ_p:

$$C_p(t) = \frac{\langle \mathbf{X}_p(t) \cdot \mathbf{X}_p(0) \rangle}{\langle \mathbf{X}_p(0) \cdot \mathbf{X}_p(0) \rangle} = \exp\left(-\frac{t}{\tau_p}\right). \tag{4.16}$$

For $p = 1, 2, 3, 5, 9, 17$ the values of $C_p(t)$ for systems with different stiffness ($N = 35$) are shown in Fig. 4.13. The general trend, in qualitatively agreement with the semiflexible chain model of Harnau et al. (1999), is the increase of the mode relaxation time when

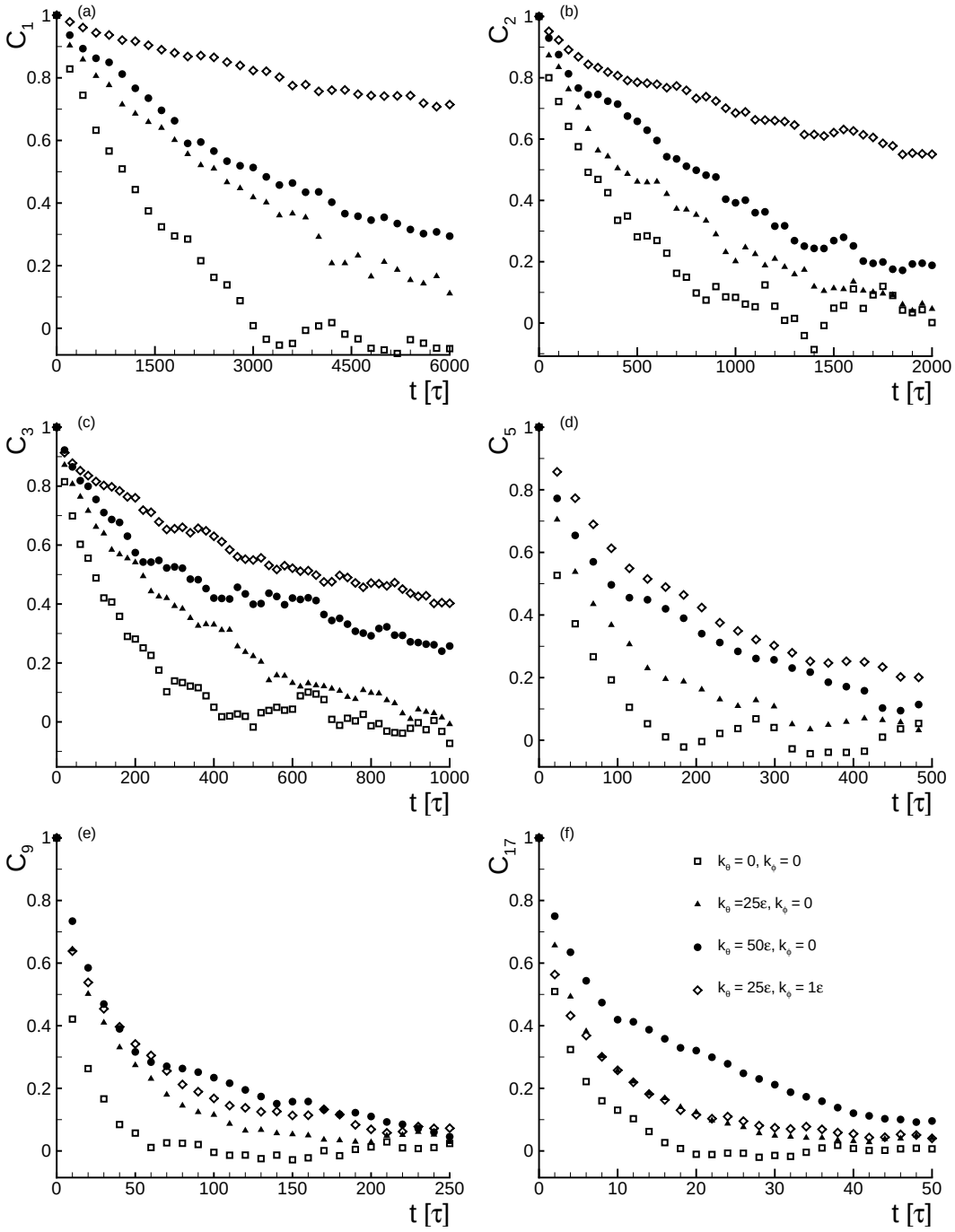

Figure 4.13: *Normalized autocorrelation functions of Rouse modes, $C_p(t)$ for p = 1, 2, 3, 5, 9, 17 ((a)–(f)) vs. time in melts with $N = 35$ beads. The chain stiffness, characteristic for all pictures, is indicated in (f).*

the stiffness is enhanced, indicating a change in effective bead friction as emphasized before. At the smaller scale we notice how the torsion influence vanishes because the scattered wave length is smaller than the distance between any bead i and $i+3$.

Consistent with the approximation of the relaxation time τ_p: $\tau_p^{-1} = W\lambda_{\mathrm{p}} \approx p^2/N^2$, we found that, for flexible chains, the plots of $\ln C_p$ vs. tp^2/N^2, for all mode numbers p approximately collapse onto a master curve. This scaling behavior is not much affected by the bending stiffness (for all modes) and torsion stiffness (small modes numbers) but it vanishes for large mode numbers when torsion potential is considered.

Instead of the exponential law predicted by the Rouse model we fitted the curves in Fig. 4.13 with a stretched exponential form (Smith et al. 2001, Padding and Briels 2002, Padding and Briels 2001):

$$C_p(t) = \exp\left[-\left(\frac{t}{\tau_p^*}\right)^{\beta_p}\right] \tag{4.17}$$

where the relaxation time τ_p^* and stretching parameter β_p depend on the mode number p and on the chain length. Our findings indicate deviations from the exponential Rouse prediction ($\beta_p = 1$) as follows: $\beta_1 = 0.9$ to $\beta_{17} = 0.7$ for flexible chains and $\beta_1 = 0.8$ to $\beta_{17} = 0.5$ for the bending–torsion stiffness. So, stiffness effects are evident at the local scale of sub-sections of the chain that are directly affected by the angle potentials.

The stiffness effects can be revealed also in experiments on neutron quasi-elastic scattering by polymers, in which short wavelength scattered radiation corresponds to vibrations and viscous motion of very small sections of the chain. In MD studies, the quantity of interest is the single chain intermediate coherent structure factor:

$$S(q,t) = \frac{1}{N}\sum_{k,l}^{N}\left\langle e^{-i\mathbf{q}\cdot\mathbf{r}_k(t)}\cdot e^{i\mathbf{q}\cdot\mathbf{r}_l(0)}\right\rangle \tag{4.18}$$

From this, by applying a suitable time-Fourier transform, the directly measured single chain dynamic structure factor $S(q,\omega)$ is obtained. The average in Eq. (4.18) is done over all the chains in the melt and over 100 starting states and 20 orientations for a specific modulus q of the scattering vector $\mathbf{q}$. We restrict the investigation to large values of q (the corresponding wavelengths are smaller than the end-to-end distance and larger than the bond length) in such a way that the inelastic scattering probes the motion of the internal chain modes.

Fig. 4.14(a)–(c) shows the decay in time of the normalized structure factor,

$$S'(q,t) = \frac{S(q,t)}{S(q,0)}. \tag{4.19}$$

In the Rouse model, S' can be calculated rigorously (de Gennes 1967, Dubois-Violette and de Gennes 1967, Doi and Edwards 1989) and for the regime of interest

$$\ln S' \propto -q^2 t^{1/2}. \tag{4.20}$$

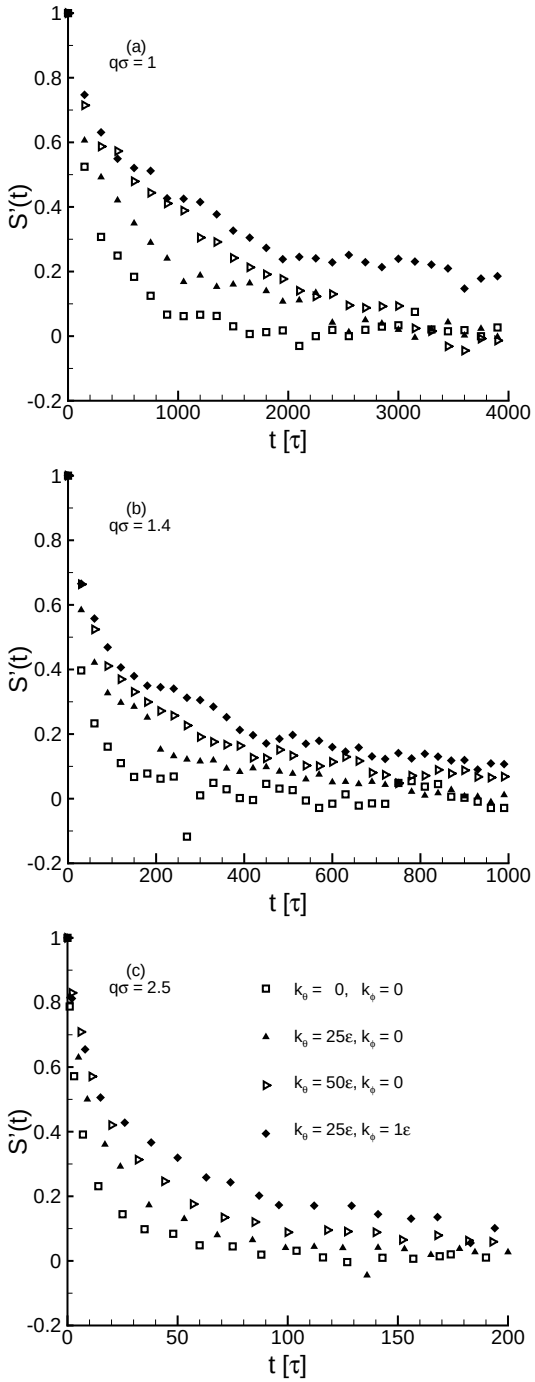

Figure 4.14: *Single chain intermediate coherent structure factor for melts with* $N = 35$, $M = 100$ *with different stiffness. The* $q\sigma$ *values are* 1 *(a),* 1.4 *(b) and* 2.5 *(c). The symbols defined in (c) apply also to (a) and (b).*

An improved dependence

$$\ln S' \propto -q^2 t^{3/4} \tag{4.21}$$

was proposed independently, first by Allegra and Ganazzoli (1981) and then by Harnau et al. (1999) as a result of two different reasons: modification of the intra-chain friction and stiffness along the chain as a result of a bending potential. An analytical structure factor expression including bending and torsion is not available at the moment. In order to decide which model matches better with our data we fit the curves from Fig. 4.14 to

$$\ln S' \propto -t^B \tag{4.22}$$

The values of B, given in Table 4.3, are in between $1/2$ and $3/4$, thus suggesting that the simulations are in between the standard Rouse model described by Eq. (4.20) and the updated one corresponding to Eq. (4.21). Quite interestingly, the time-scaling for the chains with bending and torsion are closest to the Rouse model at all considered scales.

	$q\sigma = 1$	$q\sigma = 1.4$	$q\sigma = 2.5$
$k_\theta = 0, k_\phi = 0$	0.72	0.62	0.56
$k_\theta = 25\varepsilon, k_\phi = 0$	0.62	0.57	0.61
$k_\theta = 50\varepsilon, k_\phi = 0$	0.70	0.52	0.60
$k_\theta = 25\varepsilon, k_\phi = 1\varepsilon$	0.54	0.49	0.49

Table 4.3: *The slope B from Eq. (4.22) for all cases presented in Fig. 4.14.*

Another practical way to elucidate the nature of the chain motion inside the melt is direct visualization of the chain trajectories. If the chain has a Rouse-like motion, its trajectories are isotropically spread inside the melt, but when the motion changes to reptation these trajectories should become confined inside a tube. For one randomly chosen chain from the melt, Fig. 4.15 shows the stiffness effects on the localization of the chain trajectories. The ten snapshots displayed are taken after equilibration, at equal time intervals. To eliminate the distortions induced by the time scaling, the time interval for each case is equivalent with 10% of the characteristic Rouse time τ_R estimated from Fig. 4.11.

As can be seen in Fig. 4.15(a)–(c) the motion of short chains, observed during a specific time, is not significantly affected by increasing the chain stiffness. In terms of chain trajectory localization, no "reptation tube" is formed to confine the chain as in reptation theory and the motion of stiff short chains is still Rouse-like.

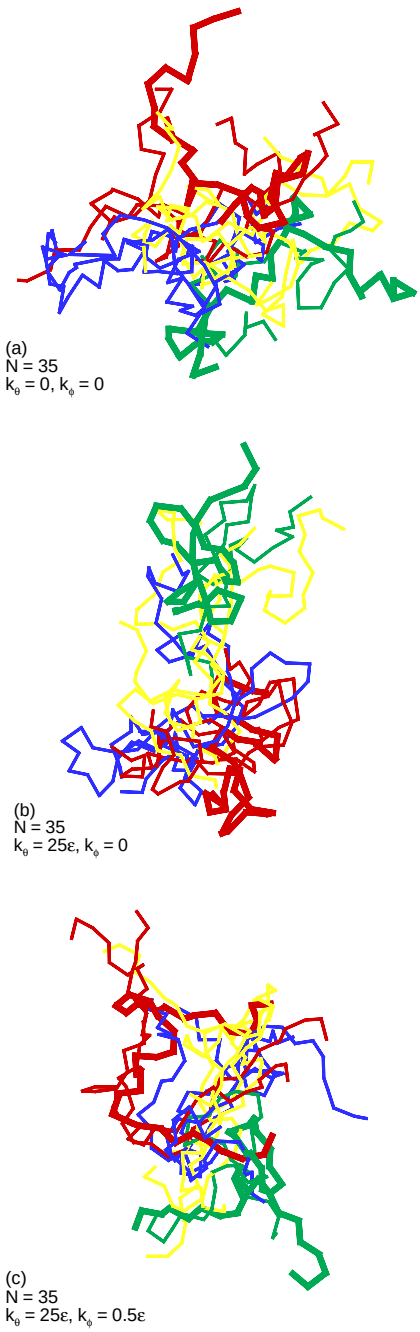

Figure 4.15: *Visualization of a randomly chosen polymer chain from the melt during a time interval equal with Rouse time τ_R. The chain is represented with distinct colors at successive equal time intervals. The thicker lines represent the first and the last snapshot from the series.*

4.5 Conclusions

This chapter has presented and discussed results from extensive MD simulations, at constant temperature and density, that investigate the effects of chain stiffness on the dependence of self-diffusion coefficient D on polymer length N.

From the D vs. N analysis we conclude that as the chain stiffness increases the conventional Rouse and reptation regimes are significantly modified: the reciprocal slope of the Rouse regime increases gradually from 1 to 2 and the slope for the reptation regime reaches the value 2.2. At the same time, the crossover between these two regimes, related with the entanglement length N_{e}, is shifted to longer chains until it becomes ill-defined. Moreover, the entanglement length N_{e} extracted from bead mean-square displacement analysis for long chains, exhibits the same increasing trend with chain stiffness. We argue that this behavior origins from the specific bending and torsion potentials used.

To investigate more carefully the nature of short chain motion, we have analyzed the bead mean-square displacement, the normal mode autocorrelation functions and the dynamic structure factor for chains with different rigidities and visualized the chain trajectories. The bead mean-square displacement, $g_1(t)$, for short chains as well as the chain visualized trajectories show moderate deviations from Rouse behavior but major differences with reptation. Also from the normal mode and structure factor analysis mentioned, we can conclude that the motion behavior of short stiff chains does not clearly obey any of the currently available theories.

The chain rigidity has been modeled by means of generic bending and torsion potentials acting along the polymer backbone. For the torsion potential we have proposed a novel form, depending on dihedral and comprised bending angles, which eliminates the computational instabilities when two consecutive bonds align. More particular expressions for these potentials, adapted to chemically detailed chain architectures, as well as specific interactions (hydrogen bonds, polar forces) are expected to further modify the chain stiffness, and therefore to affect the dynamics even more.